Article

Monthly Convective Boundary Layer Height Study over Brazil Using Radiosonde, ERA5, and COSMIC-2 Data

Gregori de Arruda Moreira [1], María Jesús Pérez Herrera [2], Ginés Garnés Morales [3,4], Maria João Costa [4], Alexandre Cacheffo [5], Samara Carbone [6], Fábio Juliano da Silva Lopes [7], Jesús Abril-Gago [2,8], Juana Andújar-Maqueda [2,8], Ediclê de Souza Fernandes Duarte [4], Vanda Cristina Pires Salgueiro [4], Daniele Bortoli [4] and Juan Luis Guerrero-Rascado [2,8,*]

1   Federal Institute of Education, Science and Technology of São Paulo (IFSP), Department of Sciences and Mathematics (DCM), São Paulo 01109-101, Brazil; gregori.moreira@ifsp.edu.br
2   Andalusian Institute for Earth System Research (IISTA-CEAMA), University of Granada, 18006 Granada, Spain; jabrilgago@ugr.es (J.A.-G.); juaniandujar@ugr.es (J.A.-M.)
3   Department of Meteorology, University of Reading, Reading RG6 6UR, UK; g.garnesmorales@pgr.reading.ac.uk
4   Center for Sci-Tech Research in Earth System and Energy—CREATE, Universidade de Évora, 7000-671 Évora, Portugal; mjcosta@uevora.pt (M.J.C.); edicle.duarte@uevora.pt (E.d.S.F.D.); vsalgueiro@uevora.pt (V.C.P.S.); db@uevora.pt (D.B.)
5   Pontal Institute of Exact and Natural Sciences (ICENP), Federal University of Uberlândia (UFU), Campus Pontal, Ituiutaba 38304-402, Minas Gerais, Brazil; cacheffo@ufu.br
6   Institute of Agricultural Sciences (ICIAG), Federal University of Uberlândia (UFU), Uberlânda 38408-100, Brazil; samara.carbone@ufu.br
7   Institute of Environmental, Chemical and Pharmaceutical Sciences (ICAQF), Federal University of São Paulo (UNIFESP), Campus Diadema, Diadema 09913-030, Brazil; fjslopes@unifesp.br
8   Department of Applied Physics, University of Granada, 18071 Granada, Spain
*   Correspondence: rascado@ugr.es

Highlights

What is the main finding?

- The Convective Boundary Layer Height (CBLH) exhibits seasonal behavior that varies with the continentality and climate to which it is exposed.

What are the implications of the main finding?

- The CBLHs can be grouped into six regions (Northern Amazon, North, Northeast, Midwest, Southeast, and South);
- The CBLHs estimated from ERA5 and COSMIC-2 data show considerable agreement for most of the year;
- The large number of forest fires in the Midwest region of Brazil causes an overestimation of the CBLH estimated from COSMIC-2 data.

Abstract

Although the atmospheric boundary layer height (ABLH) is a highly relevant parameter for various meteorological studies, the analysis of its behavior remains undersampled in South America, especially in Brazil. In this context, this work presents a monthly characterization of the ABLH during the convective period (Convective Boundary Layer Height-CBLH) using radiosonde data and a comparison between the monthly patterns obtained from ERA5 and COSMIC-2 data. The results demonstrate that, based on radiosonde data, the CBLH can be grouped into six regions (Northern Amazon, North, Northeast, Midwest, Southeast, and South), with seasonality varying according to the continentality and the climate to which they are exposed. The ERA5 and COSMIC-2 data show considerable agreement for

most of the year [average absolute difference of [362 ± 182] m] and demonstrate the same seasonality observed in radiosondes for the North Amazon, North, Northeast, Southeast, and South regions. The highest discrepancies between ERA5 and COSMIC-2 occur during the fire season, mainly at Midwest region, reaching 802 m in July, likely linked to the sensitivity of the COSMIC-2 to fire plumes.

1. Introduction

The Earth's troposphere is subdivided into two key regions, namely the Atmospheric Boundary Layer (ABL) and the free troposphere (FT). The ABL is the lowest region of the troposphere where direct interactions with the Earth's surface (land and sea) occur, so that this layer responds directly to surface forcings at timescales of less than 1 h. On the other hand, the indirect effects (e.g., in the residual layer) can extend to the daily timescale [1]. Key characteristics of the ABL include its variable extent, ranging from a few hundred meters to several kilometers, and its fluctuations between day and night, as well as with topography. This portion of the troposphere, influenced by the Earth's surface, plays a crucial role in the exchange of heat, momentum, moisture, gases, and aerosol particles between the surface and the atmosphere [2,3]. Due to its high variability depending on the different atmospheric stability regimes, the ABL has subdivisions that are directly associated with the time of day [2,3]. During the day, when convective activity dominates, the ABL is predominantly dominated by the Convective Boundary Layer (CBL). During the night, a period of greater stability and dominance of mechanical turbulence, the ABL is predominantly composed of two sublayers, namely the Stable Boundary Layer (SBL) and the Residual Layer (RL) [2]. A correct characterization of the ABL dynamics, as well as its sublayers, is fundamental for pollutant dispersion models, weather forecasting, and air quality prediction. Therefore, gaining a comprehensive understanding of this atmospheric layer and acquiring quantitative knowledge of ABL dynamics are crucial [1].

Although several studies have applied satellite [4–6], reanalysis [7,8], and radiosonde [9,10] data to characterize the ABLH globally, there is still a significant gap in studies detailing the dynamics of ABLH in the Southern Hemisphere, mainly in South America. Part of this issue is associated with the small number of monitoring stations in this Hemisphere [11–13]. Another relevant point is that tropical and subtropical climate zones are characterized by high solar radiation incidence onto the Earth's surface, driving strong convective activity, complex turbulence patterns, and significant vertical homogenizing processes, which altogether reduce atmospheric stratification. Additionally, these regions are characterized by a notable prevalence of clouds due to high humidity and intense convection fields. Consequently, the ABLH estimation in these latitudes can be challenging, as it is more variable in space and time than in other regions, and the presence of clouds complicates the use of remote sensing techniques for its retrieval [14].

Specifically in the case of Brazil, the country with the largest territorial extension in South America, the few studies related to the ABL dynamics were carried out or on Amazon region (e.g., [15]) or on urban centers (e.g., [16]), particularly on the city of São Paulo. These studies have employed, radiosondes [17] and remote sensing systems, such as elastic lidars [18–21] and Doppler lidars [22]. Possible solutions to this limitation include estimating the ABLH from Global Navigation Satellite System Radio Occultation (GNSS-RO) data or Reanalysis data. Kalmus et al. [5] estimated the ABLH from GNSS-RO data and compared these values with those obtained from radiosonde data, finding reasonable

agreement. Regarding reanalysis, Guo et al. [23] compared the ABLH estimated by four reanalysis models (ERA5, MERRA-2, JRA-55, and NCEP-2) with that calculated from radiosonde data. They demonstrated that ERA5 provides the best agreement with the lowest bias.

In this context, the present study investigates the monthly variation in the average CBLH across Brazil. Firstly, the CBLH estimated from historical radiosonde data will be presented on the available sites (spots). Then, COSMIC-2 data will be used to estimate the CBLH with greater spatial coverage. These results will also be compared with those generated by the ERA5 reanalysis model in order to potentially increase the temporal extension with greater spatial coverage. Both datasets are compared with seasonal behavior described by radiosonde data.

This article is then organized as follows. The analyzed regions and the experimental setup are described in Section 2. The applied methodologies are introduced in Section 3. In Section 4 the results are presented. Then, finally the conclusions are given in Section 5.

2. Materials and Methods

2.1. Study Area

Brazil is the largest country in Latin America, occupying nearly half of the South American continent (47.3%) and ranking as the fifth-largest country in the world. It spans an area of 8.5 million km^2 and extends approximately from 5° N to 30° S latitude and from 74° W to 35° W longitude. Additionally, the country has a population that exceeds 200 million and is composed of 26 federated states and the Federal District [24]. These states can be grouped into five main regions based on their thermal behavior throughout the year, namely the North, Northeast, Midwest, Southeast, and South regions [25].

Due to Brazil's location and vast size, the equator passes through the northern region of the country, very close to Macapá, the capital of the state of Amapá. At the same time the Tropic of Capricorn crosses the southern region near the city of São Paulo. In addition, the country spans four time zones, ranging from UTC-2 to UTC-5. These characteristics enhance the difficulty of performing meteorological and climatological studies in this country, despite their undoubted relevance.

Brazilian Topography and Climate

The Brazilian landscape does not feature major mountain ranges and is predominantly characterized by plateaus, plains, and depressions. This type of terrain makes Brazil a low-altitude country, with 41% of its territory lying below 200 m asl (a fact that is most notable in the Amazon River basin and the Pantanal of Mato Grosso), and only 7% above 800 m asl, concentrated in the eastern and southeastern regions near the Atlantic Ocean [26].

Additionally, Brazil exhibits diverse climatic zones due to its size, geographic location, and topography. According to Köppen's climate classification conducted by [27], Brazil has three primary climatic zones: tropical, semi-arid, and subtropical. The tropical climate zone is the largest, covering 81.4% of the Brazilian territory and present across almost all regions of the country. Meanwhile, the semi-arid climate is characteristic of the northeastern region, encompassing nearly 5% of the territory, and the subtropical climate is typical of the southern region, accounting for 13.7% of the total area. The subtropical climate dominates south of the Tropic of Capricorn, while the tropical climate prevails north of it.

However, Brazil's territory exhibits a significant climatic diversity within each zone mentioned above. Considering the average annual temperature patterns, the regions shown in Figure 1 are characterized as follows: the northern region is consistently warm and humid, with minimal seasonal variations. In contrast, the northeastern region is marked by high temperatures and periods of drought (semi-arid climate). The Midwest

region experiences high temperatures during the austral spring and summer, with slightly milder temperatures in autumn and winter. The southeastern region acts as a transition zone between the warm climate of the lower latitudes and the temperate climate of the mid-latitudes. Lastly, the southern region is dominated by a temperate (subtropical) climate with significant temperature fluctuations throughout the year [26].
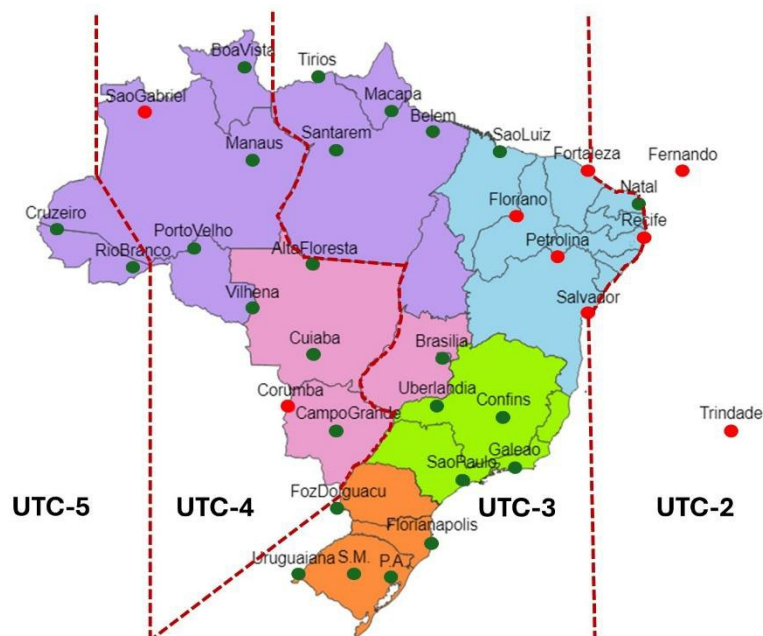
Figure 1. Map of Brazil divided into states and regions (Violet—North; Blue—Northeast; Pink—Midwest; Green—Southeast; Orange—South) with the initially selected stations. SM refers to the Santa Maria station, and PA refers to the Porto Alegre station. The dark green dots represent the stations considered in this study, while the red dots represent the removed stations due low data availability.

2.2. Instruments and Datasets

For this study, radiosonde data from the National Oceanic and Atmospheric Administration (NOAA), refractivity profiles obtained by the Constellation Observing System for Meteorology, Ionosphere and Climate (COSMIC-2), and data from the ECMWF Reanalysis v5 (ERA5) were utilized. All the datasets used are free to the public, accessible, and can be retrieved through [28–30].

2.2.1. Radiosonde

The NOAA maintains a global collection of atmospheric records acquired through radiosonde launches. This collection is known as the Integrated Global Radiosonde Archive (IGRA) and includes over 2800 stations distributed worldwide. In Brazil, IGRA contains records from 62 stations, of which 30 are currently operational [31]. Figure 1 shows a map of Brazil divided into states and regions, highlighting the preselected stations.

The radiosonde model currently used in Brazil is the RS92-SGP, manufactured by Vaisala. This equipment provides vertical profiles of temperature, relative humidity, pressure, wind speed, and direction, with associated uncertainties of ±0.5 °C, $\pm5\%$, ±1.0 hPa, ±0.15 m/s, and $\pm2°$, respectively. Soundings are conducted at 12:00 UTC at all stations, while some stations, particularly those located in the Southeast and South regions, also perform soundings at 00:00 UTC.

However, in this study, only stations with more than 70% total data availability and more than 60% availability in each month between 2008 and 2023 at 12 UTC (dark green dots–Figure 1) were considered. This strategy avoids the inclusion of stations with long

periods of missing data, which could introduce bias into the analysis. Therefore, the stations of São Gabriel, Fortaleza, Fernando, Floriano, Recife, Petrolina, Salvador, Corumbá, and Trindade (red dots–Figure 1) were removed from the analyses presented in the next sections, yielding a total of 25 stations used.

2.2.2. Constellation Observing System for Meteorology Ionosphere and Climate 2 (COSMIC-2)

In addition to radiosondes, this study has employed atmospheric data obtained by COSMIC-2, a satellite constellation launched into space on 25 June 2019, with data availability starting on October 1 of the same year. The constellation consists of six satellites that orbit the Earth around the equator at an altitude of about 720 km [32]. Their orbit is tilted at 24° so that the measurements from COSMIC-2 focus on the undersampled tropical and subtropical regions between 45°N and 45°S, where tropospheric activity is more complex and intense [6,33].

To retrieve vertical profiles of atmospheric variables such as temperature, pressure, and air humidity, COSMIC-2 analyzes the refraction of radio signals emitted by GPS satellites. When radio waves enter the Earth's atmosphere, they refract proportionally to the air's humidity and pressure, and inversely proportional to temperature. This change in trajectory is known as GNSS-Radio Occultation, and with it, COSMIC-2 can approximately obtain seven refractivity profiles per day in a $5° \times 5°$ region, which translates into more than 4000 high-quality height-resolved profiles per day [34].

2.2.3. European Centre for Medium-Range Weather Forecasts Reanalysis v5 (ERA-5)

ERA5 is the fifth generation of global atmospheric reanalysis produced by the European Centre for Medium-Range Weather Forecasts (ECMWF). Reanalysis data results from combining historical and real-time meteorological observations from various sources around the world, such as weather stations, radiosondes, and satellites, with numerical prediction models. This combination provides coherent atmospheric data with greater spatial homogeneity. To integrate the observations into numerical models, ERA5 uses the 4D-Var data assimilation method, which minimizes the differences between observations and the model to determine the initial conditions of the atmosphere. Additionally, the numerical prediction model employed is the Integrated Forecasting System (IFS) in version CY41R2 [33].

The ERA5 reanalysis dataset spans from January 1940 to the present and is updated daily with a 5-day delay. It provides global coverage on a regular grid with a horizontal spatial resolution of 0.25° (approximately 31 km) for atmospheric variables. The atmosphere is resolved using 137 vertical model levels (from the surface to 80 km altitude) and 37 pressure levels (from 1000 to 1 hPa), offering hourly information on numerous variables along with uncertainty estimates [33]. Additionally, ERA5 also provides single-level meteorological data, which are 2D data corresponding to a single level of the atmosphere, typically the surface.

3. Methods

3.1. CBLH Estimated from Radiosonde Data

Following the methodology used by [35,36], the CBLH can be estimated using radiosondes through the parcel method (PM) [36] (Figure 2). This method also defines the CBLH as the height to which an air parcel at room temperature can rise adiabatically from the ground by convection, or equivalently, the height z at which the potential temperature $\theta(z)$ equals the surface potential temperature $\theta(z_0)$.
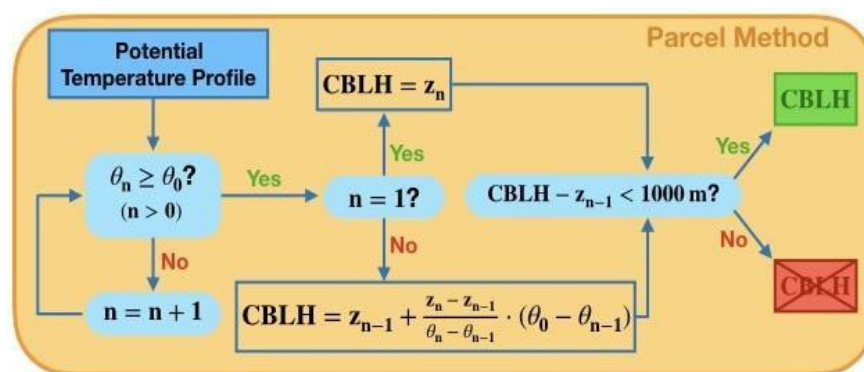
Figure 2. Scheme of the algorithm applied to radiosondes under convective situations.

As illustrated in the flowchart in Figure 2, the potential temperature profile is first evaluated for instability. When instability is found ($\theta(z_n)$), the CBLH is determined via a linear interpolation between the z_n and the preceding levels, due to the low vertical resolution of radiosonde data. As an additional quality control, values for which the difference with the previous height (z_{n-1}) exceeds 1000 m (threshold defined empirically) are discarded to avoid overestimation.

3.2. ABLH Estimated from COSMIC-2 Data

The atmospheric refractivity (*N*) refers to the ability of air to refract a wave, which varies based on its composition or density. More specifically, in the troposphere, where the presence of water vapor is significant, *N* can be expressed as a function of air temperature, pressure, and partial vapor pressure, as follows [6]:

$$N = 77.6\frac{P}{T} + 3.73 \cdot 10^5 \frac{e}{T^2} \quad , \tag{1}$$

where *P* is the air pressure [hPa], *T* is the temperature [K], and *e* is the partial pressure of water vapor [hPa].

The COSMIC-2 refractivity profiles exhibit a high penetration into the troposphere (more than 50% reach 200 m agl [37]), so one of the main objectives of this satellite constellation is to study the ABLH.

In the ABL region, there is generally a sharp variation in temperature and/or humidity with height [37]. These changes are associated with a considerable decrease in refractivity (Equation (1)), so studying its gradient makes it possible to detect the ABLH. Through refractivity, the ABLH can be determined using two methods: (i) the refractivity gradient method (RGM) [6] and (ii) the threshold method (Lowest Significant Gradient Method, LSGM) [37]. On the one hand, the RGM identifies the ABLH at the absolute minimum of the refractivity gradient. On the other hand, the LSGM defines the ABLH as the minimum below the RGM that has a certain significant percentage of its magnitude (generally 80%). If more than one minimum meets the established condition, the method considers the lowest minimum as the ABLH. If no minimum below the RGM reaches the required magnitude, the threshold method coincides with the gradient method. The LSGM is useful in tropical and subtropical regions where other factors, such as the presence of low clouds or moisture advection, can generate refractivity minima similar to or even greater than the ABLH.

In this work, the CBLH study over Brazil was conducted by applying the LSGM to COSMIC-2 refractivity profiles, which are obtained from the COSMIC-2 wetPf2 level 2 files. Such files contain the atmospheric occultation profile, with humidity information included, interpolated to 100 m height levels. The CBLH estimation was carried out using an algorithm developed by [6], who, after conducting an investigation of the ABLH with

different instruments and comparing their results with the refractivity profiles, concluded that the optimal percentages or thresholds for applying the LSGM are those listed in Table 1, which presents thresholds based on the type of surface (land or ocean) and the period (day, night, or transitions, i.e., sunrise and sunset).

Table 1. Thresholds applied in the LSGM following [6].

Surface	Period	Threshold
Land	Day	82%
	Night	68%
	Transition	98%
Ocean	All	99%

Before applying the LSGM to the N profiles of wetPf2 files all profiles with a minimum height of more than 500 m are discarded to reduce the risk of overestimating the CBLH value. Then, the mean value of the latitude and longitude profiles from ground level to a height of 4 km is calculated, and this value is attributed as the representative coordinates for each profile. Finally, using the mean latitude and longitude coordinates of each file and the date, it calculates the solar declination angle to determine the UTC times of sunrise and sunset. So, it classifies each file according to the period of the day to which they belong (day, night, or transition), considering the transition period to be the interval between ± 1.5 h around sunrise and sunset. Once all these steps have been executed, the algorithm estimates the value of the CBLH by applying the threshold method and the percentages shown in Table 1, and finally, represents for each period its monthly average value (in meters agl) on a map with $1° \times 1°$ resolution using the Python package PyGMT (v0.017.0) [38].

3.3. ABLH Estimated from ERA5 Data

The ABLH provided by ERA5 is estimated from the bulk Richardson number (R_{ib}) [39]. Ref. [40] evaluated numerous methods for estimating the ABLH and found that the bulk Richardson number method proposed by [41] was the most appropriate for radiosonde data, reanalysis data, and climate models due to its validity in both stable and unstable situations, its lack of negative heights, and its lack of strong dependence on vertical resolution. From a physical perspective, the R_{ib} is a dimensionless number that measures the ratio of buoyancy-associated turbulence to mechanical turbulence caused by wind shear, and can be described as follows:

$$R_{ib}(z) = \frac{g \cdot [\theta_v(z) - \theta_v(z_0)] \cdot [z - z_0]}{\theta_v(z_0) \cdot \left[(u(z) - u(z_0))^2 + (v(z) - v(z_0))^2\right]} \; , \tag{2}$$

where g is the acceleration of gravity, z_0 is the height of the location (above sea level), θ_v is the virtual potential temperature, and u and v are the zonal and meridional wind components, respectively. Both the CBLH and SBLH can be determined as the altitude where the R_{ib} reaches the critical value of 0.25. More details can be found in [42]. The ERA5 ABLH is provided with a grid resolution and temporal resolution of $0.25° \times 0.25°$ and 1 h, respectively.

To compare the ERA5 data with the experimental measurements from COSMIC-2, the algorithm described in Section 3.2 was implemented to calculate the difference in the mean CBLH values at each point on the map with a $1° \times 1°$ resolution. This enables comparison of the two databases for different times of the day (day, night, and transition). For the sake of reducing computational time, the ERA5 data were resampled to a spatial resolution of $1.5° \times 1.5°$ and a temporal resolution of 2 h, respectively. Finally, the difference in the mean CBLH values were mapped for each period of the day and month of the year with a $1.5° \times 1.5°$ resolution.

4. Results and Discussion

4.1. Characterization of CBLH from Radiosonde Data

Figure 3 illustrates the monthly CBLH value at 12 UTC from 2008 to 2023 for the 25 stations analyzed in this work. Each point represents the geographic location of the station, with its color indicating the mean CBLH monthly value. On the other hand, the dot size is associated with the standard deviation; therefore, smaller points indicate low variability, while larger ones are associated with greater variability concerning the monthly mean value.
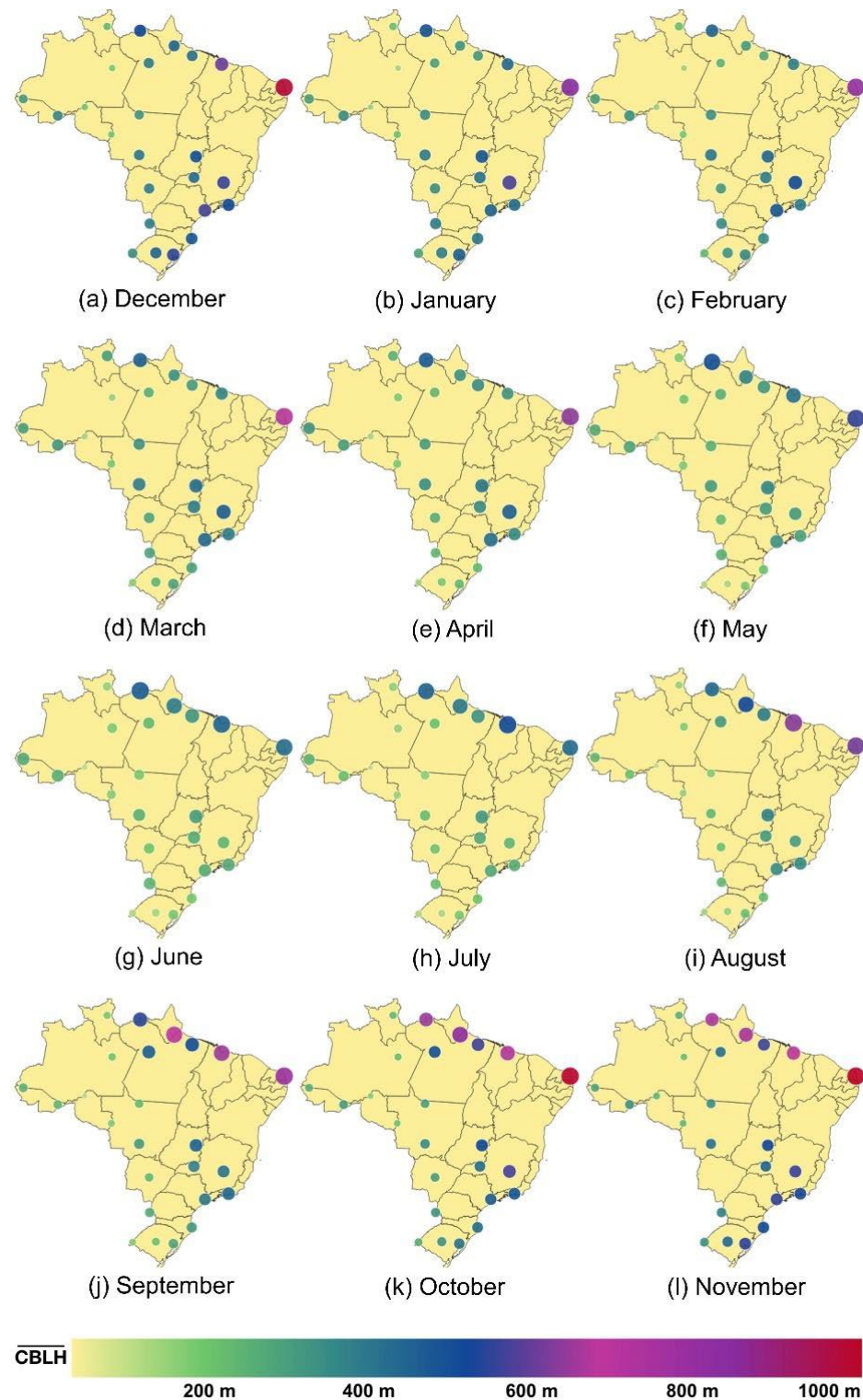
Figure 3. CBLH monthly average ($\overline{CBLH}$), at 12:00 UTC, of all analyzed stations from 2008–2023.

In general, all the analyzed stations demonstrate seasonality, albeit with distinct characteristics. It is important to highlight that due to different Brazilian Time Zones, Figure 3 illustrates different moments of the CBLH evolution. This factor is associated with the vast extension of Brazilian territory, which encompasses several latitudes [5° N to 33° S], longitudes [35° W to 75° W], and time zones [UTC-5 to UTC-2]. Furthermore, this country is endowed with different biomes (Caatinga [composed by species adapted to water scarcity, with thorny trees and shrubs], Atlantic Forest [high biodiversity and dense vegetation], Cerrado [poor and acidic soils, and vegetation composed of shrubs and grasses], Pantanal [extensive flooded areas with sandy soils and rich biodiversity], Amazon [presence of the largest tropical forest in the world with large rivers], and Pampa [predominance of grasses and herbaceous plants]), climates and topographies. In addition, it is important to highlight that the stations of the same regions can have different continentalities (e.g., Galeão, located in the coastal region, and Confins, situated approximately 550 km from the sea, both in the Southeast region). The two stations with the highest monthly average values are located in the North [Macapá (805 ± 271) m in October] and Northeast [Natal with (1078 ± 319) m in November], the Brazilian regions presenting the highest mean temperatures, highlighting Natal station, which has the highest CBLH values throughout much of the year. On the other hand, the two stations endowed with the smallest average monthly values (lower than 200 m) are observed in the South region (the region with the lowest mean temperatures) [Uruguaiana with (86 ± 50) m in May] and the North region close to the Amazon (Amazon North) [Porto Velho (58 ± 35) m in July], which is endowed with high humidity. This characteristic can make the air more stable and consequently result in lower CBLH values at 12 UTC.

Figure 4 presents the $\overline{CBLH}$ values grouped by regions. However, the North region was subdivided into two parts (Amazon North and North) due to the strong influence of the Amazon biome and climate on the CBLH dynamics. In general, the division shown in Figure 4 effectively groups regions with similar seasonal behavior, as well as the periods of maximum and minimum values. The exception is the Northeast region, which will be discussed subsequently.

The stations located in the Amazon North (Figure 4a) exhibit relatively constant values, with minimum and maximum ones recorded in July and December/January, respectively. The station located in Porto Velho stands out for having the lowest average values, not exceeding 200 m throughout the year. On the other hand, the Rio Branco station has the highest average values, ranging between 200 and 350 m during the year, with the maximum value in December ([336 ± 197] m). It is important to note that, as previously mentioned, this group of stations exhibits a special behavior in comparison with other ones located in the North region, given the intense influence of the Amazon climate, which has high humidity throughout the year [27] and results in low values for the $\overline{CBLH}$.

The stations in the North region (Figure 4b) are influenced by the equatorial climate, which has two characteristic seasons, the wet (from December to May) and the dry (from June to November) [27], when the higher $\overline{CBLH}$ values are predominantly observed, mainly between September and November. Macapá is the station that reaches the highest monthly average value ([805 ± 207] m in October), while Boa Vista registered the lowest values in almost all months, surpassing 200 m only in three months (March [270 ± 239] m, April [218 ± 207] m and November [223 ± 208] m). Similar behavior was also observed by [10].

The stations in the Midwest (Figure 4c), South (Figure 4e), and Southeast (Figure 4f) regions show similar average CBLH behavior, both among stations within the same region and among different regions. Such behavior can be associated with the occurrence of well-defined and similar seasons in three regions, so that both have a summer with high temperatures and pluviosity (December to February) and a winter endowed with the lowest

temperatures and pluviosity (June to August) [27]. Overall, the mean CBLH height does not exceed 600 m (the maximum average monthly value is observed in Confins station, $[553.9 \pm 291.6]$ m, during October). Furthermore, in these areas, the seasonal variation in the mean CBLH is more moderate than in the northeast. However, slightly greater variability is observed in the south and southeast compared to the center-west. In the latter, the average annual amplitude is about 100 m, while in the first two, it reaches 250 m, depending on the season. This behavior and range of values, in Southeast stations, were also observed by [21] using lidar and radiosonde data, and [10] applying only radiosonde data.
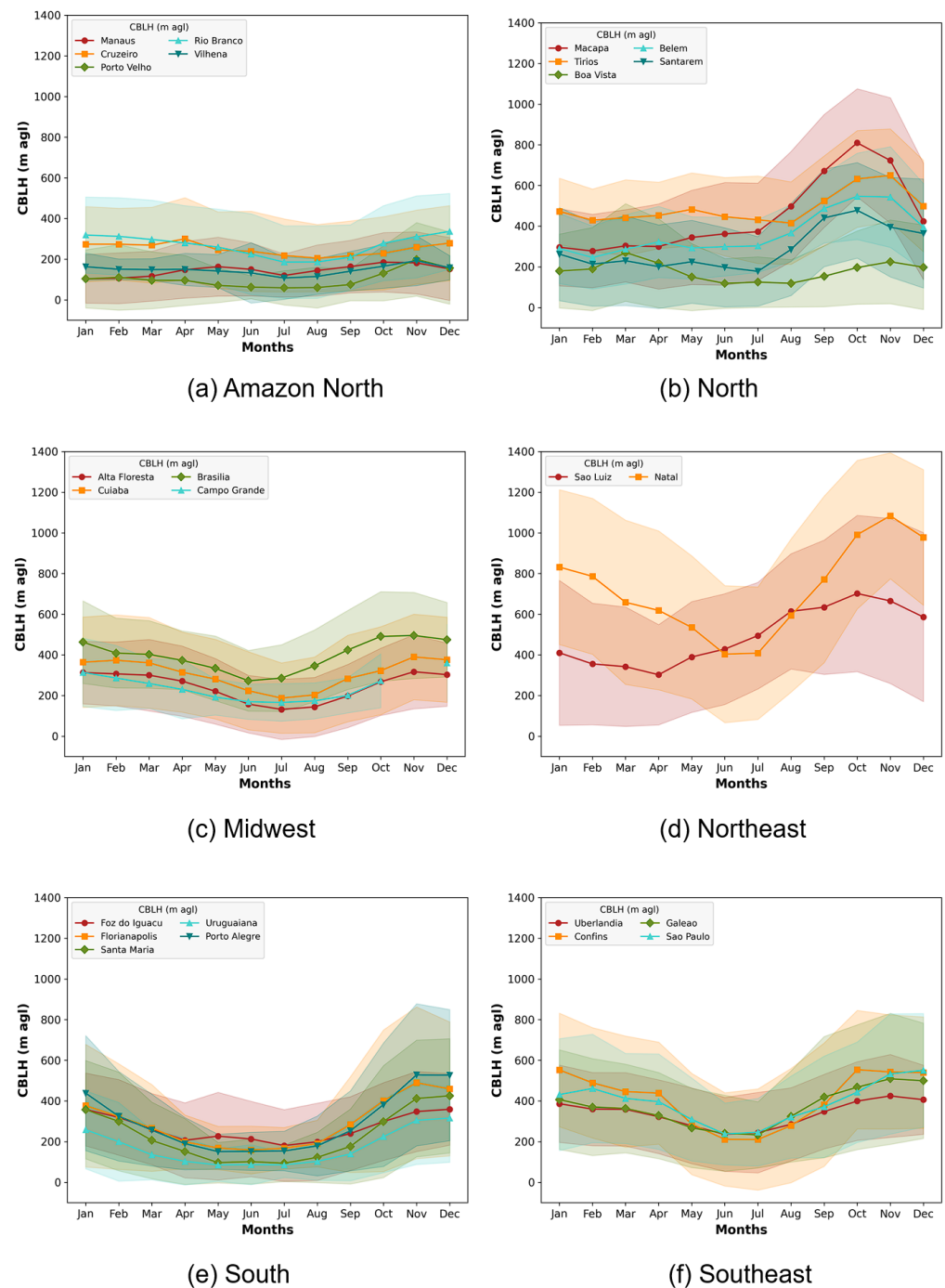
Figure 4. CBLH monthly average ($\overline{CBLH}$) and its standard deviations (shadows), at 12:00 UTC, of all analyzed stations from 2008 to 2023, grouped by regions (**a**) Amazon North, (**b**) North, (**c**) Midwest, (**d**) Northeast, (**e**) South, and (**f**) Southeast.

Despite the agreement shown by the CBLH behavior with the regional division of the stations presented in Figure 4, there is a notable discrepancy between the results from the two Northeastern stations (Figure 4d). Although both belong to the same region, the São Luís station is located in the geographic north of Brazil, closer to the Belém station (approximately 580 km away) than to the Natal station (around 1400 km away). For this reason, the mean CBLH in São Luís shows behavior more similar to that of the northern stations, while the CBLH in Natal reflects behavior perhaps more in line with the semi-arid climate characteristic of the northeast region, varying from the minimum average value of [403.6 ± 337.0] m in June, to maximum average value of [1078.0 ± 319.9] m in November.

Supplementary Table S1 and Figure 5 present the monthly average, as well as its respective standard deviation, and median values, for all analyzed stations. Comparing the median and average values it is possible to identify the variability in altitudes within a single month. Stations located in the northern Amazon have the least variability (mean and median values close to each other). Conversely, the greatest variability is observed at stations in the Northeast region (Natal from January to March and São Luíz from October to December), at the Santarém station (North Region) from January to May, and at the Florianópolis station (South Region) from June to August.

4.2. Comparison Between the CBLH Estimated from COSMIC-2 and ERA5

Figure 6 presents the monthly average CBLH value obtained from COSMIC-2 data ($\overline{CBLH}_{COSMIC-2}$). It is important to note that, unlike what is presented in Figure 3, where all values given represent the CBLH at the same hour (12 UTC), Figure 6 displays the average CBLH value obtained from all COSMIC-2 overpasses that occurred during the daily period. Consequently, the average values in Figure 5 are higher than those presented in Figure 4, so that the regional pattern is not clearly defined, as could be observed in the previous section.

The Amazon North and the North continue having the lowest average values, which agrees with Figure 4. On the other hand, the highest values (around 3000 m) are observed in the Midwest region from July to September.

COSMIC-2 refractivity measurements are obtained through Radio Occultation (RO) signals, so they are subject to one of the main problems experienced by this type of data: their sensitivity to duct or trapping layers. These are layers where the refractive index drops sharply, causing the inversion method that calculates refractivity from RO signals to fail and generate lower values than expected. The presence of these layers is more common in tropical regions and can be caused by sudden changes in temperature and humidity profiles [6]. Furthermore, ref. [43] found during the Australian wildfires of 2019 and 2020 that the appearance of duct layers for communication signals is partly caused by the smoke plumes from those fires. This fact could explain the anomalies found in the COSMIC-2 results, as they coincide with the dry season and, therefore, with the annual forest fire season in Brazil, which runs from June to September [44]. Consequently, fire debris is likely influencing the determination of CBLH through refractivity profiles and LSGM. Similar results were also observed by [6], who observed CBLH values around 2500 m in the JJA period.

Figure 7 shows the monthly average CBLH values provided by ERA5 for the entire Brazilian territory. The results for the North, North Amazon, Northeast, and South regions present the same seasonality observed in Figure 3, so that the maximum and minimum periods observed in that figure correspond to those in Figure 7. It is important to highlight that, as in Figure 6, the values shown are the monthly averages of all values provided for the daytime period; therefore, the amplitudes are higher than those retrieved by radiosondes at 12 UTC.
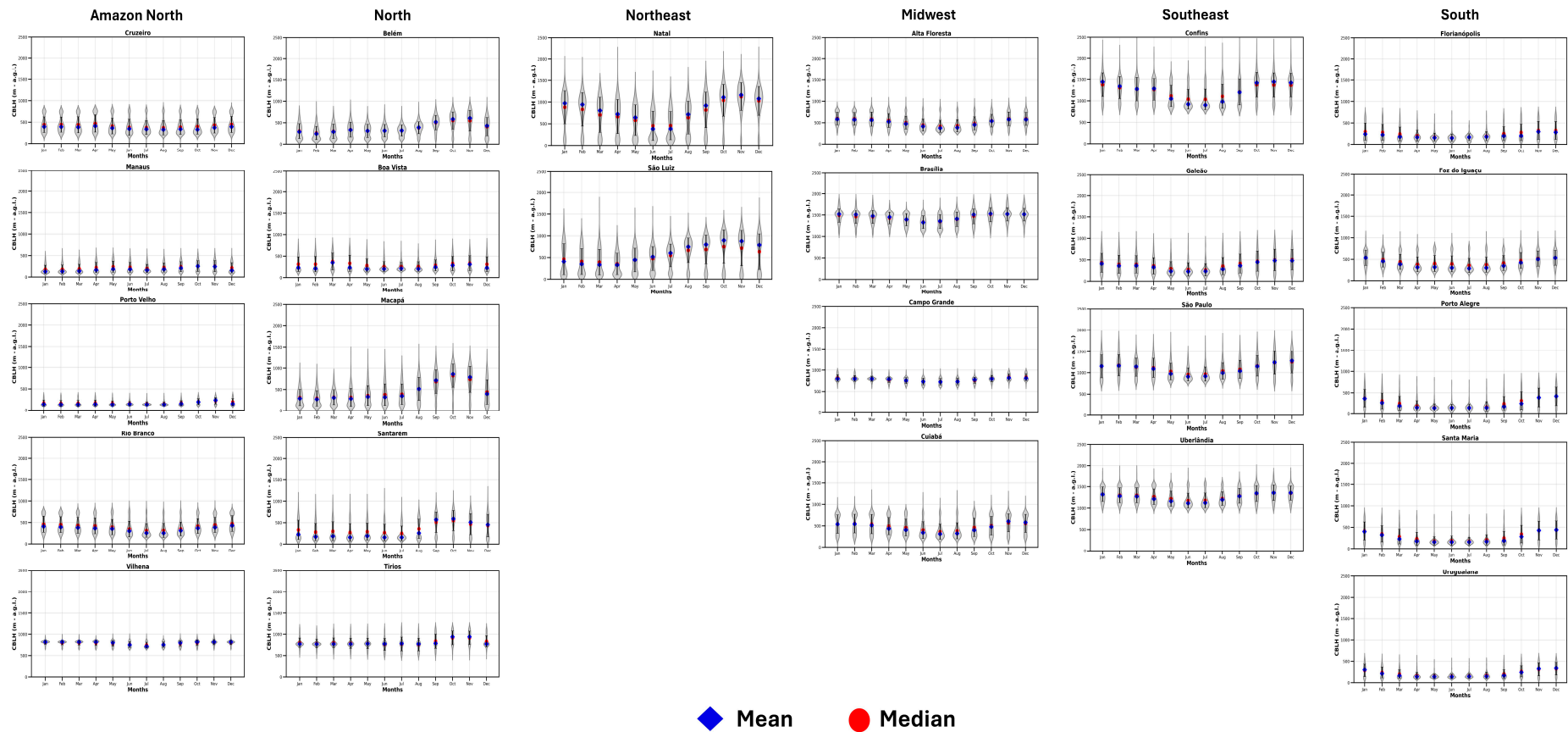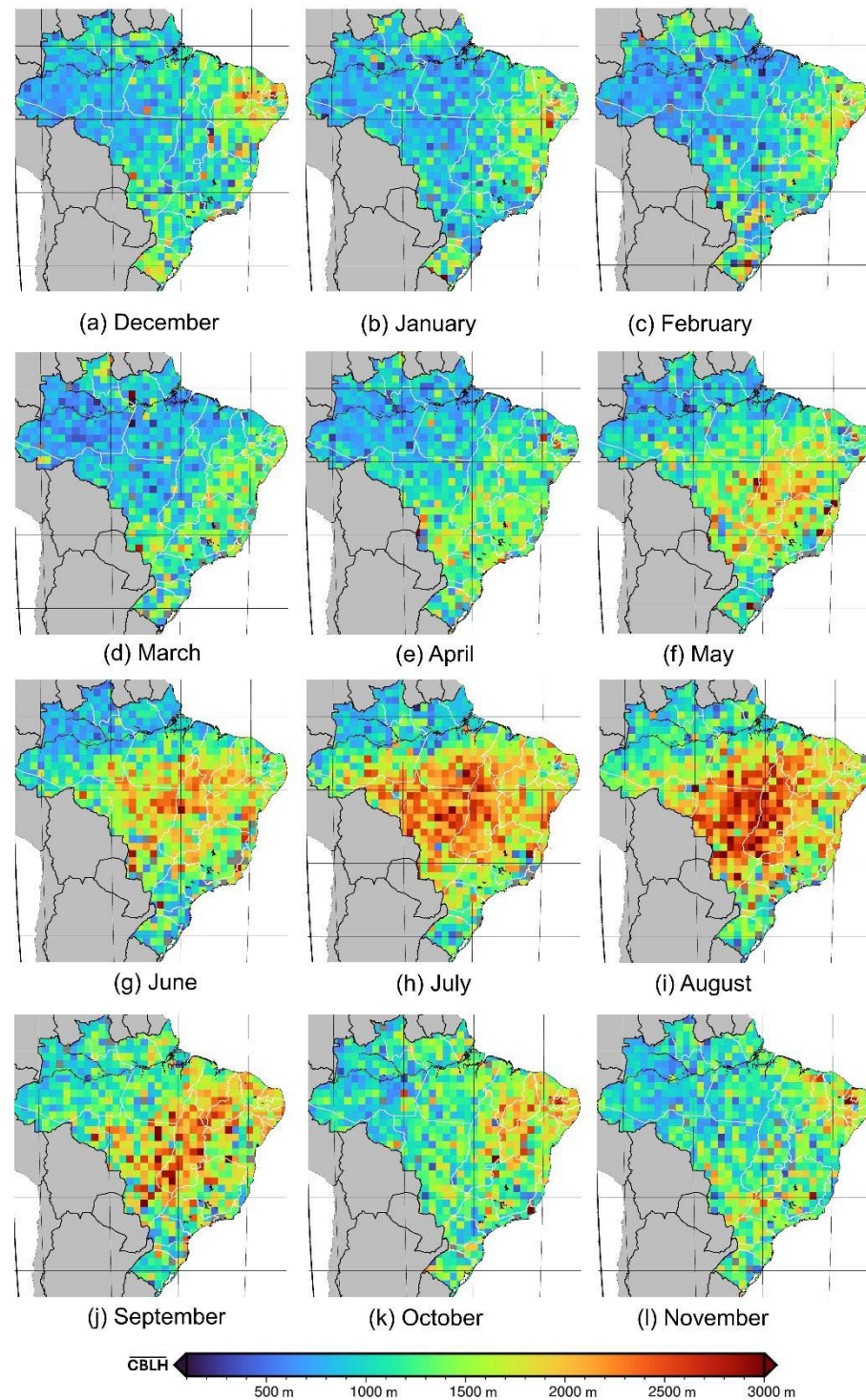
**Figure 5.** Data distribution, Mean (blue diamond), Median (red circle) for all analyzed stations.

Figure 6. CBLH monthly average obtained from COSMIC-2 data ($\overline{CBLH}_{COSMIC-2}$) from October 2019 to December 2023.

The Midwest presents a behavior different from that observed from radiosonde data, so that from July until September, this region reaches the highest CBLH values on Brazilian territory. In accordance with radiosondes, the lowest values of CBLH in the Midwest occur between June and August.
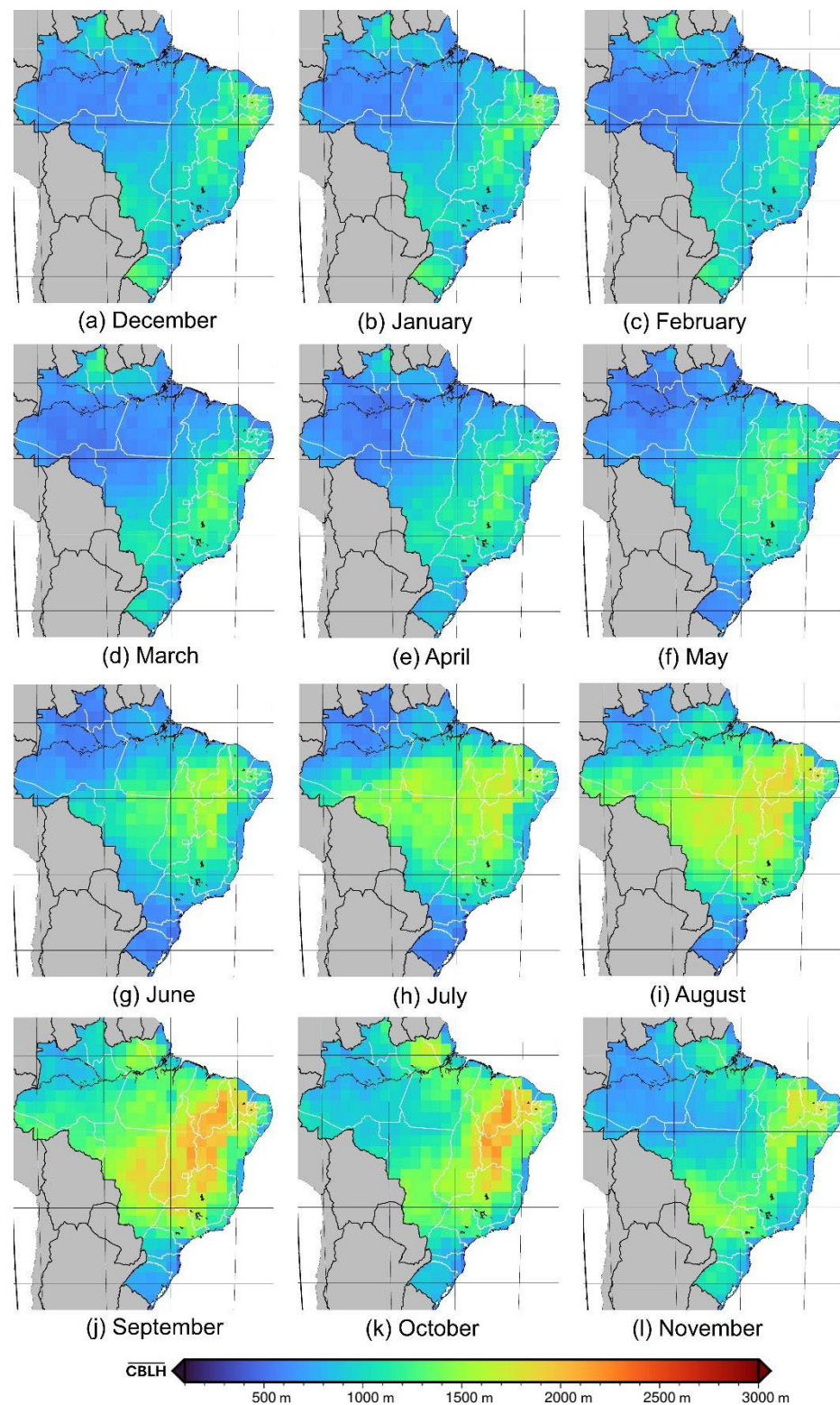
Figure 7. CBLH monthly average obtained from ERA5 data ($\overline{CBLH}_{ERA5}$) from October 2019 to December 2023.

Supplementary Figure S1 demonstrates the monthly difference between $\overline{CBLH}_{COSMIC-2}$ and $\overline{CBLH}_{ERA5}$. From this figure, it is possible to conclude that the average results from COSMIC-2 and ERA5 are very similar during the daily period, as expected, except between May and August (mainly July and August, forest fire season) in the Midwest, Southeast, and South regions. Such differences are highlighted in Table 2, where it is possible to observed that the highest differences between $\overline{CBLH}_{COSMIC-2}$ and $\overline{CBLH}_{ERA5}$ occur in

July for all regions, so that the two highest values are 802 and 757 m for the Midwest and South regions. However, although $\overline{CBLH}_{COSMIC-2}$ is higher in these areas during these months, Figure 6 also demonstrates an increase of $\overline{CBLH}_{ERA5}$ in the Midwest region, mainly in July and August. The similarity between the monthly behavior of the mean values for COSMIC-2 and ERA5 may be because since 25 March 2020, ECMWF has been using COSMIC-2 observations for its weather forecasts and data assimilation (https://www.ecmwf.int/en/newsletter/163/news/ecmwf-starts-assimilating-cosmic-2-data (accessed on 5 September 2024)). Furthermore, COSMIC-2 focuses on tropical and subtropical regions, offering greater coverage and observations in these regions than other satellites that also provide RO signals, such as COSMIC-1 [45], CHAMP, or GRACE [46]. Thus, its impact on these regions is more significant.

Table 2. Monthly average difference between $\overline{CBLH}_{COSMIC-2}$ and $\overline{CBLH}_{ERA5}$ per Brazilian region.

Brazilian Regions	MAE (M) ($CBLH_{COSMIC-2}$-$CBLH_{ERA5}$)											
	JAN	FEB	MAR	APR	MAY	JUN	JUL	AUG	SEP	OCT	NOV	DEC
North	179	171	169	200	290	311	355	285	143	130	178	183
Northeast	416	423	367	328	442	530	533	525	418	382	320	376
Midwest	60	149	111	271	561	634	802	727	230	50	128	63
Southeast	241	270	306	480	646	606	661	537	256	213	274	294
South	288	407	430	516	565	508	757	517	426	420	354	320

This argument is reinforced by [5], which shows the ABLH estimated by the ERA-Interim model (previous version of ERA5). This model assimilated data from COSMIC-1, whose coverage did not focus on tropical regions, and its results do not reflect the unusually high values for the southern hemisphere winter in central Brazil. Furthermore, ref. [6] evaluated the impact of COSMIC-2 on ERA5 water vapor profiles in tropical and subtropical regions and found that measurements from this satellite constellation significantly affected the data provided by the model.

Therefore, the comparison between COSMIC-2 and ERA5 measurements during the daytime period reflects the impact of assimilating COSMIC-2 observations into the ERA5 model. While both datasets show overall good agreement (is lower than 300 m in around 42% of the year), situations where CBLH from COSMIC-2 is overestimated (such as during forest fire events) do not produce the same overestimation in ERA5.

5. Conclusions

The average CBLH results obtained from radiosondes offer a more precise and regional view of the behavior of this variable. Furthermore, these records have confirmed that the average CBLH responds consistently to different climates, topography, and continentality.

In the northern region, there are two distinct CBLH behaviors: one at stations near the equator, where the CBLH remains constant throughout the year until the months of dry season, when it experiences a significant increase; and another at stations closer to the Amazon (Amazon North), where the CBLH remains constant throughout the year, with minimal variations, and not exceeding 500 m in height. On the other hand, the northeast region records the highest average CBLH values, especially in the austral summer months, where they exceed 1000 m. Furthermore, this region presents the most significant seasonal amplitude between winter and summer. Finally, it is observed that the average CBLH behavior is quite similar in the midwestern, southeastern, and southern regions, where the variation between winter and summer is more moderate than in the northeast.

The CBLH estimated from COSMIC-2 and ERA5 provides a more general perspective on the monthly behavior of CBLH for all Brazilian territory. The results from both are consistent with seasonal patterns observed via radiosondes for the North Amazon, North, Northeast, South, and Southeast regions. However, for the Midwest region, there is a significant discrepancy between June and September, particularly in the results generated by COSMIC-2. The LSGM used in the COSMIC-2 measurements is sensitive to possible changes in the threshold that determines the ABLH, which may be caused by the presence of different atmospheric layers or by the presence of aerosol particle layers, such as fire debris, which are very frequent in the Midwest region from June to August (fire season). In addition, this similarity demonstrates that COSMIC-2 observations have a significant impact on the ERA5 ABLH reanalysis data.

Abbreviations

The following abbreviations are used in this manuscript:

ABL   Atmospheric Boundary Layer

ABLH	Atmospheric Boundary Layer Height
FT	Free Troposphere
CBLH	Convective Boundary Layer Height
SBLH	Stable Boundary Layer Height
RL	Residual Layer
GNSS-RO	Global Navigation Satellite System Radio Occultation
NOAA	National Oceanic and Atmospheric Administration
COSMIC-2	Constellation Observing System for Meteorology, Ionosphere and Climate
ERA5	ECMWF Reanalysis v5
IGRA	Integrated Global Radiosonde Archive
IFS	Integrated Forecasting System
RGM	Refractivity Gradient Method
LSGM	Lowest Significant Gradient Method

References

1. Kotthaus, S.; Bravo-Aranda, J.A.; Collaud Coen, M.; Guerrero-Rascado, J.L.; Costa, M.J.; Cimini, D.; O'Connor, E.J.; Hervo, M.; Alados-Arboledas, L.; Jiménez-Portaz, M.; et al. Atmospheric boundary layer height from ground-based remote sensing: A review of capabilities and limitations. *Atmos. Meas. Tech.* **2023**, *16*, 433–479. [CrossRef]
2. Garratt, J.R. Review: The atmospheric boundary layer. *Earth-Sci. Rev.* **1994**, *37*, 89–134. [CrossRef]
3. Stull, R.B. *An Introduction to Boundary Layer Meteorology*; Atmospheric and Oceanographic Sciences Library; Springer: Dordrecht, The Netherlands, 1988.
4. Zhang, W.; Guo, J.; Miao, Y.; Liu, H.; Zhang, Y.; Li, Z.; Zhai, P. Planetary boundary layer height from CALIOP compared to radiosonde over China. *Atmos. Chem. Phys.* **2016**, *16*, 9951–9963. [CrossRef]
5. Kalmus, P.; Ao, C.O.; Wang, K.N.; Manzi, M.P.; Teixeira, J. A high-resolution planetary boundary layer height seasonal climatology from GNSS radio occultations. *Remote Sens. Environ.* **2022**, *276*, 113037. [CrossRef]
6. Garnés-Morales, G.; Costa, M.J.; Bravo-Aranda, J.A.; Granados Muñoz, M.J.; Salgueiro, V.; Abril Gago, J.; Fernández Carvelo, S.; Andújar Maqueda, J.; Valenzuela, A.; Foyo Moreno, I.; et al. Four Years of Atmospheric Boundary Layer Height Retrievals Using COSMIC-2 Satellite Data. *Remote Sens.* **2024**, *16*, 1632. [CrossRef]
7. von Engeln, A.; Teixeira, J. A Planetary Boundary Layer Height Climatology Derived from ECMWF Reanalysis Data. *J. Climate* **2015**, *26*, 6575–6590. [CrossRef]
8. Yang, S.S.; Pan, C.J. Climatology of the Atmospheric Boundary Layer Height Using ERA5: Spatio-Temporal Variations and Controlling Factors. *Atmosphere* **2025**, *16*, 573. [CrossRef]
9. Seidel, D.J.; Ao, C.O.; Li, K. Estimating climatological planetary boundary layer heights from radiosonde observations: Comparison of methods and uncertainty analysis. *J. Geophys. Res.* **2010**, *115*, D16113. [CrossRef]
10. Gu, J.; Zhang, Y.; Yang, N.; Wang, R. Diurnal variability of the planetary boundary layer height estimated from radiosonde data. *Earth Planet. Phys.* **2020**, *4*, 479–492. [CrossRef]
11. Guerrero-Rascado, J.L.; Landulfo, E.; Antuña, J.C.; Barbosa, H.M.J.; Barja, B.; Bastidas, A.E.; Bedoya, A.E.; da Costa, R.F.; Estevan, R.; Forno, R.; et al. Latin American Lidar Network (LALINET) for aerosol research: Diagnosis on network instrumentation. *J. Atm. Solar-Terr. Phys.* **2016**, *138–139*, 112–120. [CrossRef]
12. Antuña-Marrero, J.C.; Landulfo, E.; Estevan, R.; Barja, B.; Robock, B.A.; Wolfram, E.; Ristori, P.; Clemesha, B.; Simonich, D.; Zaratti, F.; et al. LALINET: The first Latin American-born regional atmospheric observational network. *Bull. Amer. Meteorol. Soc.* **2017**, *98*, 1255–1275. [CrossRef]
13. Reid, K.J.; Arblaster, J.M.; Alexander, L.V.; Siems, S.T. Spurious trends in high latitude Southern Hemisphere precipitation observations. *Geophys. Res. Lett.* **2024**, *51*, e2023GL106994. [CrossRef]
14. Krishnamurti, T.N.; Stefanova, L.; Misra, V. *Tropical Meteorology: An Introduction. Springer Atmospheric Sciences*, 1st ed.; Springer New York: New York, NY, USA, 2013.
15. Carneiro, R.G.; Fisch, G. Observational analysis of the daily cycle of the planetary boundary layer in the central Amazon during a non-El Niño year and El Niño year (GoAmazon project 2014/5). *Atmos. Chem. Phys.* **2020**, *20*, 5547–5558. [CrossRef]
16. Saraiva, L.; Krusche, N. Estimation of the Boundary Layer Height in the Southern Region of Brazil. *Am. J. Environ. Eng.* **2013**, *3*, 63–70. [CrossRef]

17. Piñero Sánchez, M.; de Oliveira, A.P.; Varona, R.P.; Tito, J.V.; Codato, G.; Ribeiro, F.N.D.; Marques Filho, E.P.; Silveira, L.C.d. Rawinsonde-based analysis of the urban boundary layer in the metropolitan region of São Paulo, Brazil. *Earth Space Sci.* **2019**, *7*, e2019EA000781. [CrossRef]

18. Moreira, G.A.; da Silva Andrade, I.; Cacheffo, A.; da Silva Lopes, F.J.; Calzavara Yoshida, A.; Gomes, A.A.; da Silva, J.J.; Landulfo, E. Influence of a Biomass-Burning Event in $PM_{2.5}$ Concentration and Air Quality: A Case Study in the Metropolitan Area of São Paulo. *Sensors* **2021**, *21*, 425. [CrossRef] [PubMed]

19. Moreira, G.A.; Oliveira, A.P.D.; Codato, G.; Sánchez, M.P.; Tito, J.V.; Silva, L.A.H.E.; Silveira, L.C.D.; Silva, J.J.D.; Lopes, F.J.D.S.; Landulfo, E. Assessing Spatial Variation of PBL Height and Aerosol Layer Aloft in São Paulo Megacity Using Simultaneously Two Lidars during Winter 2019. *Atmosphere* **2022**, *13*, 611. [CrossRef]

20. Moreira, G.A.; Pereira Oliveira, A.; Piñero-Sánchez, M.; Codato, G.; da Silva Lopes, F.J.; Landulfo, E.; Pereira Marques Filho, E. Performance assessment of aerosol-lidar remote sensing skills to retrieve the time evolution of the urban boundary layer height in the Metropolitan Region of São Paulo City, Brazil. *Atmos. Res.* **2022**, *277*, 106290. [CrossRef]

21. Moreira, G.A.; Amorim Marques, M.T.; da Silva Lopes, F.J.; Andrade, M.F.; Landulfo, E. Analyzing the influence of the planetary boundary layer height, ventilation coefficient, thermal inversions, and aerosol optical Depth on the concentration of $PM_{2.5}$ in the city of São Paulo: A long-term study. *Atmos. Pollut. Res.* **2024**, *15*, 102179. [CrossRef]

22. Marques, M.T.A.; Moreira, G.A.; Pinero, M.; Oliveira, A.P.; Landulfo, E. Estimating the planetary boundary layer height from radiosonde and Doppler Lidar measurements in the city of São Paulo—Brazil. *EPJ Web Conf.* **2018**, *176*, 06015. [CrossRef]

23. Guo, J.; Zhang, J.; Yang, K.; Liao, H.; Zhang, S.; Huang, K.; Lv, Y.; Shao, J.; Yu, T.; Tong, B.; et al. Investigation of near-global daytime boundary layer height using high-resolution radiosondes: First results and comparison with ERA5, MERRA-2, JRA-55, and NCEP-2 reanalyses. *Atmos. Chem. Phys.* **2021**, *21*, 17079–17097. [CrossRef]

24. Ministério de Assuntos Exteriores (Governo do Brasil): Dados Sobre Geografia do Brasil. Available online: https://www.gov.br/mre/pt-br/embaixada-bogota/datos-sobre-brasil/geografia (accessed on 19 August 2024).

25. Ministério de Assuntos Exteriores, União Européia e Cooperação (Gobierno de España): Ficha País Brasil. Available online: https://www.exteriores.gob.es/Documents/FichasPais/BRASIL_FICHA%20PAIS.pdf (accessed on 19 August 2024).

26. Alvares, C.A.; Stape, J.L.; Sentelhas, P.C.; Gonçalves, J.L.d.M. Modeling monthly mean air temperature for Brazil. *Theor. Appl. Climatol.* **2013**, *113*, 407–427. [CrossRef]

27. Alvares, C.A.; Stape, J.L.; Sentelhas, P.C.; de Moraes Gonçalves, J.L.; Sparovek, G. Köppen's climate classification map for Brazil. *Meteorol. Z.* **2013**, *22*, 711–728. [CrossRef]

28. IGRA Sounding Data for the Full Period of Record. Available online: https://www.ncei.noaa.gov/data/integrated-global-radiosonde-archive/access/data-por/ (accessed on 17 July 2024).

29. COSMIC-2 Data. Available online: https://data.cosmic.ucar.edu/gnss-ro/cosmic2/nrt/ (accessed on 17 July 2024).

30. ERA5: Download Data. Available online: https://cds.climate.copernicus.eu/datasets/reanalysis-era5-single-levels?tab=download (accessed on 17 July 2024).

31. Durre, I.; Yin, X.; Vose, R.S.; Applequist, S.; Arnfield, J. Enhancing the Data Coverage in the Integrated Global Radiosonde Archive. *J. Atmos. Ocean. Technol.* **2018**, *35*, 1753–1770. [CrossRef]

32. Schreiner, W.S.; Weiss, J.P.; Anthes, R.A.; Braun, J.; Chu, V.; Fong, J.; Hunt, D.; Kuo, Y.-H.; Meehan, T.; Serafino, W.; et al. COSMIC-2 Radio Occultation Constellation: First Results. *Geophys. Res. Lett.* **2020**, *47*, e2019GL086841. [CrossRef]

33. Zhang, Z.; Xu, T.; Gao, F.; Wang, S.; Li, S. Analysis of cosmic-2 atmospheric boundary layer detection ability. In *China Satellite Navigation Conference (CSNC 2021) Proceedings, Lecture Notes in Electrical Engineering*; Springer: Singapore, 2021; pp. 43–53.

34. Ho, S.; Anthes, R.A.; Ao, C.O.; Healy, S.; Horanyi, A.; Hunt, D.; Mannucci, A.J.; Pedatella, N.; Randel, W.J.; Simmons, A.; et al. The COSMIC/FORMOSAT-3 Radio Occultation Mission after 12 Years: Accomplishments, Remaining Challenges, and Potential Impacts of COSMIC-2. *Bull. Am. Meteorol. Soc.* **2020**, *101*, E1107–E1136. [CrossRef]

35. Moreira, G.A.; Guerrero-Rascado, J.L.; Bravo-Aranda, J.A.; Benavent-Oltra, J.A.; Ortiz-Amezcua, P.; Román, R.; Bedoya-Velásquez, A.; Landulfo, E.; AladosArboledas, L. Study of the planetary boundary layer by microwave radiometer, elastic lidar and Doppler lidar estimations in Southern Iberian Peninsula. *Atmos. Res.* **2018**, *213*, 185–195. [CrossRef]

36. Moreira, G.A.; Guerrero-Rascado, J.L.; Bravo-Aranda, J.A.; Foyo-Moreno, I.; Cazorla, A.; Alados, I.; Lyamani, H.; Landulfo, E.; Alados Arboledas, L. Study of the planetary boundary layer height in an urban environment using a combination of microwave radiometer and ceilometer. *Atmos. Res.* **2020**, *240*, 104932. [CrossRef]

37. Santosh, M. Estimation of daytime planetary boundary layer height (PBLH) over the tropics and subtropics using COSMIC-2/FORMOSAT-7 GNSS–RO measurements. *Atmos. Res.* **2022**, *279*, 106361. [CrossRef]

38. Tian, D.; Leong, W.J.; Fröhlich, Y.; Grund, M.; Schlitzer, W.; Jones, M.; Toney, L.; Yao, J.; Tong, J.-H.; Magen, Y.; et al. *PyGMT: A Python Interface for the Generic Mapping Tools, v0.17.0*; Zenodo: Genève, Switzerland, 2025. [CrossRef]

39. Hersbach, H.; Bell, B.; Berrisford, P.; Hirahara, S.; Horányi, A.; Muñoz-Sabater, J.; Nicolas, J.; Peubey, C.; Radu, R.; Schepers, D.; et al. The ERA5 global reanalysis. *Q. J. R. Meteorol. Soc.* **2020**, *146*, 1999–2049. [CrossRef]

40. Zhang, Y.; Gao, Z.; Li, D.; Li, Y.; Zhang, N.; Zhao, X.; Chen, J. On the computation of planetary boundary-layer height using the bulk Richardson number method. *Geosci. Model Dev.* **2014**, *7*, 2599–2611. [CrossRef]

41. Hanna, S.R. The thickness of the planetary boundary layer. *Atmos. Environ.* **1969**, *3*, 519–536. [CrossRef]

42. Available online: https://www.ecmwf.int/sites/default/files/elibrary/2017/17736-part-iv-physical-processes.pdf#section.3.10 (accessed on 17 July 2024).

43. Abram, N.J.; Henley, B.J.; Sen Gupta, A.; Lippmann, T.J.R.; Clarke, H.; Dowdy, A.J.; Sharples, J.J.; Nolan, R.H.; Zhang, T.; Wooster, M.J.; et al. Connections of climate change and variability to large and extreme forest fires in southeast Australia. *Commun. Earth Environ.* **2021**, *2*, 8. [CrossRef]

44. Moreira, G.A.; Carbone, S.; Guerrero-Rascado, J.L.; Andrade, I.D.S.; Cacheffo, A.; Vélez-Pereira, A.M.; Zamora-Ledezma, E.; Thielen, D.; Gomes, A.A.; Duarte, E.D.S.F.; et al. Evidence of the consequences of the prolonged fire season on air quality and public health from 2024 São Paulo (Brazil) data. *Sci. Rep.* **2025**, *15*, 28337. [CrossRef] [PubMed]

45. Basha, G.; Ratnam, M.V. Identification of atmospheric boundary layer height over a tropical station using high-resolution radiosonde refractivity profiles: Comparison with GPS radio occultation measurements. *J. Geophys. Res.* **2009**, *114*, D16101. [CrossRef]

46. von Engeln, A.; Teixeira, J.; Wickert, J.; Buehler, S.A. Using CHAMP radio occultation data to determine the top altitude of the Planetary Boundary Layer. *Geophys. Res. Lett.* **2005**, *32*, L06815. [CrossRef]